

A Novel Lithium-Ion Battery Impedance Fast Measurement Method With Enhanced Excitation Signal

Xinghao Du¹, Jinhao Meng¹, Member, IEEE, Jichang Peng¹, and Youbo Liu¹, Member, IEEE

Abstract—Online battery impedance acquisition is of increasing interest due to its valuable information for state estimation and fault diagnosis. The pseudorandom sequence (PRS) can significantly mitigate the required time cost, yet suffers from an insufficient signal-to-noise ratio. Motivated by this, this article proposes a novel series-connected dual pseudorandom sequence for enhancing the signal power content in all frequency ranges, which notably improves the robustness of broadband impedance acquisition against interference. A weighted bilateral impedance filter is further carried out on a semilogarithm scale to process the measurement data, which effectively compensates for the noise-induced biases and enables a nearly unbiased result. Experimental studies verify the proposed framework by comparing it with the conventional PRS method in terms of accuracy and robustness under various states of charges, ambient temperatures, and aging status of the batteries.

Index Terms—Dual pseudorandom sequence, impedance measurements, Lithium-ion battery.

I. INTRODUCTION

LITHIUM-ION batteries have drawn massive attention in electric vehicles (EVs) and smart grid applications due to their high power and energy densities, long cycle life, and low self-discharge rate. For ensuring the batteries work within a safe and appropriate condition, a well-designed battery management system is desired to monitor batteries' states in real time [1], [2]. However, the estimation of the state of charge (SOC), state

Manuscript received 15 September 2022; revised 12 November 2022 and 15 December 2022; accepted 26 December 2022. Date of publication 9 January 2023; date of current version 9 June 2023. This work was supported in part by the National Science Foundation of China under Grant 52107229, and in part by the Fundamental Research Funds for the Sichuan Science and Technology Program under Grant 2021YJ0063 and Grant 2022YFG0123, and in part by the Fund of Robot Technology Used for Special Environment Key Laboratory of Sichuan Province under Grant 20kfkt01. (Corresponding author: Jinhao Meng.)

Xinghao Du and Youbo Liu are with the College of Electrical Engineering, Sichuan University, Chengdu 610017, China (e-mail: duxinghao@stu.scu.edu.cn; liuyoubo@scu.edu.cn).

Jinhao Meng is with the School of Electrical Engineering, Xi'an Jiaotong University, Xi'an 710049, China (e-mail: jinhao@scu.edu.cn).

Jichang Peng is with the Smart Grid Research Institute, Nanjing Institute of Technology, Nanjing 211167, China (e-mail: pengjichang@njit.edu.cn).

Color versions of one or more figures in this article are available at <https://doi.org/10.1109/TIE.2023.3234127>.

Digital Object Identifier 10.1109/TIE.2023.3234127

of health (SOH), and internal battery temperature remains a challenging task due to the strong nonlinearity [3] and sampling noise [4].

It has been reported that battery impedance has prominent dependencies on SOC [5], aging status [6], and thermal effects [7]. The low-frequency impedance represents the solid-phase and the liquid-phase diffusion processes [8], which can be used for SOC and SOH estimation [9]. In the mid-frequency range, battery impedance is dominated by charge transfer and kinetic effects, which brings valuable information concerning SOC, SOH [10], internal temperature [11], and lithium plating detection [12]. The Ohmic resistance and inductance are mainly reflected in the high-frequency region. The high-frequency impedance has been regarded as a promising tool for analyzing the battery degradation process [13], internal temperature estimation [14], and nondestructive internal heating [15]. Electrochemical impedance spectroscopy (EIS) comprehensively characterizes battery impedance at different frequency ranges using the frequency response analysis (FRA) [16]. However, the conventional EIS measurement techniques suffer from the drawback of inefficiency, the impedance measurement takes quite a long time, especially in the low-frequency region [17].

Within this context, an efficient yet easy-implementable excitation signal is necessary for realizing the onboard impedance acquisition. As shown in Fig. 1, sine-sweep [18], multisine [19], step [20], square wave [21], and pseudorandom sequence (PRS) [22], [23], [24] are the most commonly adopted signals for broadband impedance measurement. Among others, the sine-sweep signal concentrates the signal power at one fundamental frequency. In this way, the signal-to-noise ratio (SNR) can be maximized, which brings the highest measurement accuracy. The disadvantage of the sine-sweep signals, however, is that they need a long time, especially for low frequencies. For simplicity, Qahouq et al. [25] replaced the sinusoidal excitation with the square-sweep signal, while it still requires quite a long time for signal injection. To obtain the dynamic frequency responses, a fast and accurate impedance acquisition method is essential [26]. Angelis et al. [19] used a multisine signal, which greatly shortens the time cost for broadband impedance measurements. However, the sum-of-sine signal has to be designed with numerous amplitude levels, which complicates the injection process. Consequently, finite-level signals are quite preferred for their simplicity and easy-implementable property. Wang et al. [20] used a step perturbation for determining the battery impedance.

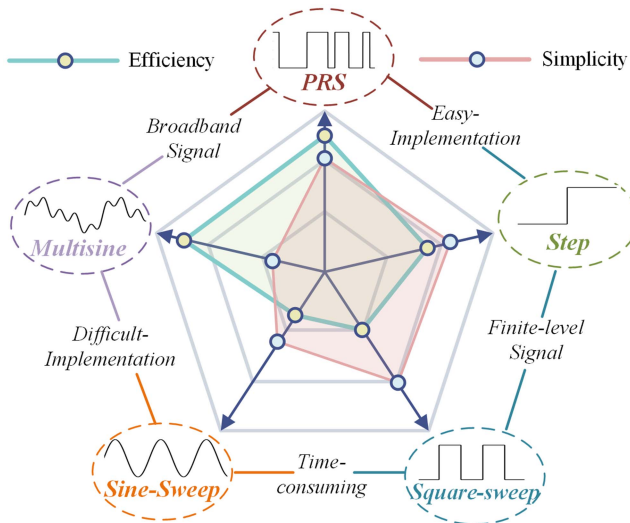


Fig. 1. Comparison of different types of the signals for broadband impedance measurements.

The step disturbance has a nonuniform power spectrum, while a lot of its power redundantly concentrates on the fundamental harmonic. In contrast, the PRS signal has a uniform power spectrum that suits broadband battery impedance measurement. Besides, the sequence can be designed with a minimum of two amplitude levels, which simplifies its implementation to a system [23]. The PRS signal combines the merits of simplicity and efficiency for online implementation and thus is further investigated in this work.

Despite all these merits mentioned above, one prominent drawback of the PRS signal is that the harmonics in the PRS signal have a low power content, which is rather susceptible to noise disturbances and further leads to biased results. The power content of the PRS signal can be improved either by increasing the amplitude or reducing the length of the sequence [27]. However, the amplitude level of the excitation signal is restricted by hardware design, and a large amplitude also elicits severe overpotential problems and nonlinear distortions [11]. Meanwhile, a short sequence length limits the frequency resolution of the PRS signal, as well as the measurable bandwidth in the low-frequency region.

Some efforts have been directed toward alleviating the above issues. For example, Sun et al. [28] used a low-pass filter (LPF) to deal with the high-frequency oscillations coming from the voltage and current sensors. However, the LPF only has a limited capability in coping with the irregular sampling noise. Liebhart et al. [29] proposed a weighted overlapped segment averaging (WOSA) method to smooth the impedance measurements. However, it requires a group of carefully designed parameters for ensuring the filtering performance, which is inconvenient in practice. Alternatively, battery impedance has a piecewise linear characteristic, which enables the linear filters to suppress noise disturbances. Sihvo et al. [23], [24] proposed a moving average filter (MAF) for smoothing the impedance measurements, which has been proven to be applicable on a 2.5-Ah LiFePO₄ battery. Nevertheless, the MAF performs questionably in presence of the

measurement data with a large variation, while the large biases that existed in the low-frequency region have not been well dealt with.

The PRS signal considerably mitigates the required time and complexity for broadband measurements, however, an inadequate signal power content could easily degrade impedance measurements' accuracy. The contradiction between the measurable bandwidth and the SNR of the PRS signal for measuring the battery impedance remains a severe problem that has not been well emphasized in previous studies. Potential challenges still lie in dealing with the large impedance biases in the low- and high-frequency ranges and acquiring trustworthy broadband impedance measurement results.

This article addressed the above issues by proposing a novel dual pseudorandom sequence (DPRS) for broadband impedance acquisition, where two subsequences are connected in series and carried out in different scales. Advanced weighted bilateral impedance filter (WBIF) based on signal power spectrum and impedance distribution is designed to process the impedance measurement data. The validity of the proposed method is verified experimentally by comparing it with the traditional PRS method and MAF for impedance filtering in terms of accuracy and robustness under various circumstances.

The main contributions of this article are summarized as follows:

- 1) A specially designed series-connected DPRS signal is proposed to greatly enlarge the signal power content in all frequency ranges, where the impedance measurements are quite robust against disturbances. Further, a WBIF is carried out on a semilogarithm scale for impedance filtering, which effectively deals with the impedance biases and enables an accurate and reliable result.
- 2) The DPRS proposed in this work greatly eases the constraints on the length of the conventional PRS signal, with the merits of high efficiency, low computational cost, and easy-implementable property that conveniently realizes rapid broadband battery impedance acquisition with high fidelity.
- 3) The proposed framework is verified to be valid and feasible on three batteries with different aging status, SOCs, and ambient temperatures providing a viable solution for future onboard impedance-based states estimation of the batteries under various operating conditions.

The remainder of this article is organized as follows. Section II elaborates on the synthesis and properties of the proposed DPRS signal. Section III details the framework of broadband battery impedance determination. Experimental results are carried out in Section IV. The main conclusions are given in Section V.

II. DUAL PSEUDORANDOM SEQUENCE

A. Pseudorandom Sequence

PRS signal has been widely employed in the field of system identification, which enables a fast and low-complexity broadband impedance measurement of the batteries. Among others, the maximum length sequence (MLS) is the most well-known class in the PRS family, which can be simply produced using a

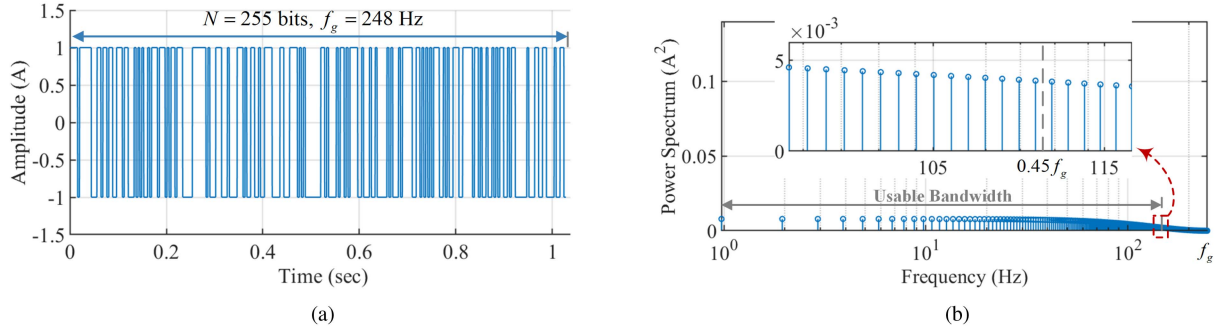


Fig. 2. Schematic representation of the PRS signal. (a) Time domain. (b) Frequency domain.

linear feedback shift register as [22]. The length N of MLS is determined by

$$N = 2^n - 1 \quad (1)$$

where $n = 1, 2, 3, \dots$ is the order of the shift register.

A schematic representation of a 255-bit-length MLS is presented in Fig. 2. In the time domain, the generating frequency of the sequence f_g is 248 Hz. The sequence only has two amplitude levels (+1, -1) that simplifies the implementation. Different from square and step disturbances, the PRS signal has near-band-limited white noise characteristics in the frequency domain and the power spectrum has a near-uniform distribution. The calculation of the PRS signal power content is given by [27]

$$P(k) = I_m^2 \frac{2(N+1)}{N^2} \left(\frac{\sin \pi k/N}{\pi k/N} \right)^2 \quad (2)$$

where $P(k)$ is the power of the k th harmonic and I_m is the amplitude of the sequence.

As shown in Fig. 2(b), the signal power content decreases toward a higher frequency, where the guideline for the maximum usable frequency is given in [23] and [30], equaling to $0.45 f_g$. The frequency resolution between the harmonics is represented as f_g/N . To ensure the PRS signal is capable of capturing battery impedance in the low-frequency region, the frequency resolution of the PRS signal has to be smaller than the minimum frequency of battery impedance. Therefore, the sequence length N is constrained by

$$N > \frac{f_g}{f_{\min}} = \frac{f_{\max}}{0.45 f_{\min}} \quad (3)$$

where f_{\max} and f_{\min} represent the maximum and minimum measurable frequencies of battery impedance. According to (2), a large N also leads to a significant reduction in signal power content, exacerbates noise interference, and further induces a biased result that cannot meet the demand of acceptable accuracy and robustness for broadband impedance acquisition. To ameliorate the above issue, a novel DPRS signal is proposed in this work.

B. Dual Pseudorandom Sequence

The proposed DPRS signal aims at improving signal power content by shortening the length of the PRS signal, which is designed with two subsequences connected in series. The

two subsequences measure the battery impedance at different frequency ranges. For the sake of brevity, the low-frequency subsequence is defined as S_{D1} and the high-frequency subsequence is S_{D2} .

Similar to the PRS signal, the proposed DPRS signal demands the frequency resolution of S_{D1} to be smaller than f_{\min} for capturing the low-frequency impedance. Therefore, the generating frequency of S_{D1} can be determined as

$$f_{g1} = f_{\min} N_1 \quad (4)$$

where N_1 is the length of S_{D1} . The maximum usable frequency of S_{D1} is represented as $0.45 f_{g1}$. For ensuring S_{D1} and S_{D2} fully cover the frequency spectrum from f_{\min} to f_{\max} , the minimum frequency of S_{D2} has to be smaller than $0.45 f_{g1}$, which is expressed as

$$f_{g2}/N_2 < 0.45 f_{g1} \quad (5)$$

where N_2 and f_{g2} are the length and generating frequency of S_{D2} . The maximum usable frequency of S_{D2} is expressed as $0.45 f_{g2}$, which also represents the maximum measurable impedance frequency

$$f_{\max} = 0.45 f_{g2}. \quad (6)$$

For the sake of uniformity in signal power spectrum, S_{D1} and S_{D2} are designed in the same length, that is, $N_1 = N_2$. By substituting (4) and (6) into (5), we can derive that N_1 and N_2 are constrained by

$$N_1 = N_2 > \sqrt{\frac{f_{g2}}{0.45 f_{\min}}} = \frac{1}{0.45} \sqrt{\frac{f_{\max}}{f_{\min}}} \quad (7)$$

where N_1 and N_2 are subjected to (1) as well.

By comparing (3) and (7), we can conclude that the proposed DPRS signal greatly eases the constraints on sequence length. By shortening N_1 and N_2 , the DPRS signal power content can be significantly improved.

Here we give an example to illustrate the property of the proposed DPRS signal. As shown in Fig. 3, the DPRS signal has the same usable bandwidth in the frequency domain as the PRS signal, where $f_{\max} = 111.6$ Hz and $f_{\min} = 1$ Hz. According to (1) and (7), N_1 and N_2 can be reduced to a minimum of 31 bits. $f_{g1} = 31$ Hz and $f_{g2} = 248$ Hz are calculated by (4) and (6). The periods of S_{D1} and S_{D2} are calculated as 1 s and 0.125 s.

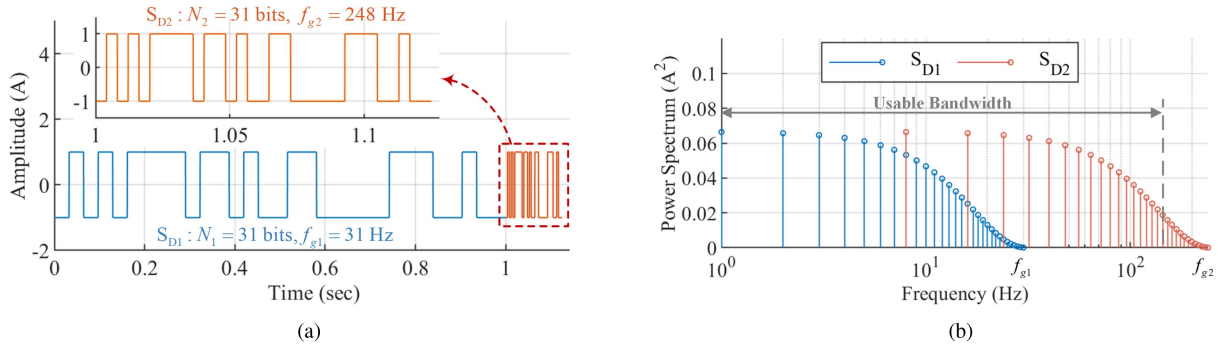


Fig. 3. Schematic representation of the proposed DPRS signal. (a) Time domain. (b) Frequency domain.

Given \$S_{D1}\$ and \$S_{D2}\$ are connected in series, \$t = 1\$ s is thus set as the division point of the subsequences.

In the time domain, the proposed DPRS signal has the same amplitude level as the PRS signal. In the frequency domain, the power content of the DPRS signal is 8.46 times larger than that of the PRS signal. In this way, the DPRS signal with an enhanced power content is considered more robust against interference and suitable for broadband battery impedance measurements. Meanwhile, the DPRS with a shorter length brings a significant reduction in the amount of the measurement data as well, thereby requiring less computing effort for signal processing and impedance determination, which is considered more convenient for practical usage.

III. IMPEDANCE DETERMINATION

The proposed DPRS signal is injected into a battery in the form of current excitation for determining the battery impedance. Considering \$S_{D1}\$ and \$S_{D2}\$ are connected in series and carried out on different scales, the measured current \$i_{D1}, i_{D2}\$, and the response voltage \$u_{D1}, u_{D2}\$ can be separately transformed into the frequency domain via discrete Fourier transform (DFT). Afterward, battery impedances \$\hat{Z}_{D1}\$ and \$\hat{Z}_{D2}\$ can be obtained using the Ohmic law as

$$\begin{cases} \hat{Z}_{D1}(f) = V_{D1}(f)/I_{D1}(f) \\ \hat{Z}_{D2}(f) = V_{D2}(f)/I_{D2}(f) \end{cases} \quad (8)$$

where \$V_{D1}(f)\$ and \$I_{D1}(f)\$ are the voltage and current harmonics correspond to \$S_{D1}\$ at the frequency \$f\$, while \$I_{D2}(f)\$ and \$V_{D2}(f)\$ correspond to \$S_{D2}\$.

Although the DPRS signal power content has been improved, biases still exist in \$\hat{Z}_{D1}\$ and \$\hat{Z}_{D2}\$ due to sampling noise and signal distortion effects. Fortunately, such noise-induced biases can be further suppressed using a specially designed WBIF to process the impedance measurement data. Notably, both \$\hat{Z}_{D1}\$ and \$\hat{Z}_{D2}\$ have a nonuniform distribution in different frequency ranges, the proposed WBIF is thus carried out on a semilogarithmic scale, which avoids constantly adjusting the filtering window. The lower and upper limits of the filtering window are defined as \$f_{i+1}\$ and \$f_{i-1}\$, which are subjected to the following equation:

$$\ln f_i = (\ln f_{i+1} + \ln f_{i-1})/2 \quad (9)$$

where \$f_i\$ is the midpoint of the filtering window.

In general, the harmonics with a higher power content are less likely to be influenced by noise disturbances, which also indicates a higher SNR. Therefore, a weighting factor is designed based on the signal power spectrum as

$$w_f = P(f) / \sum_{k=f_{i-1}}^{f_{i+1}} P(k) \quad (10)$$

where \$P(f)\$ is the power of the current harmonic at the frequency \$f\$ determined by

$$P(f) = |I(f)|^2. \quad (11)$$

Assuming battery impedance has a piecewise linear characteristic at neighboring frequencies, a bilateral filter [31] can be applied for filtering the impedance measurement data. The bilateral filter is made up of two Gaussian filters, one of which determines the weights from the impedance frequencies, where the Gaussian kernel function \$g_1\$ is defined as

$$g_1(f) = \frac{1}{\sqrt{2\pi}\sigma_f} \exp\left(-\frac{1}{2}\left(\frac{f - \mu_f}{\sigma_f}\right)^2\right) \quad (12)$$

where \$\mu_f = f_i\$, \$\sigma_f\$ is a user-defined standard deviation, which is set as six times smaller than the length of the filtering window in this work.

The other Gaussian filter calculates the weights from the distribution of the impedance measurements, where the Gaussian kernel function \$g_2\$ is defined as

$$g_2(\hat{Z}(f)) = \frac{w_f}{2\pi\sigma_{\Re}\sigma_{\Im}} \exp\left(\frac{(\Re_f - \mu_{\Re})^2}{-2\sigma_{\Re}^2} + \frac{(\Im_f - \mu_{\Im})^2}{-2\sigma_{\Im}^2}\right) \quad (13)$$

where \$\hat{Z}\$ are the measured \$\hat{Z}_{D1}\$ and \$\hat{Z}_{D2}\$ within the investigated filtering window. \$\Re_f\$ and \$\Im_f\$ are the real and imaginary parts of \$\hat{Z}(f)\$. The average values \$\mu_{\Re}\$ and \$\mu_{\Im}\$ and the standard deviations \$\sigma_{\Re}\$ and \$\sigma_{\Im}\$ are determined by

$$\begin{cases} \mu_{\Re} = \sum_{f=f_{i-1}}^{f_{i+1}} \Re_f w_f, \sigma_{\Re} = \sqrt{\sum_{f=f_{i-1}}^{f_{i+1}} w_f (\Re_f - \mu_{\Re})^2} \\ \mu_{\Im} = \sum_{f=f_{i-1}}^{f_{i+1}} \Im_f w_f, \sigma_{\Im} = \sqrt{\sum_{f=f_{i-1}}^{f_{i+1}} w_f (\Im_f - \mu_{\Im})^2} \end{cases} \quad (14)$$

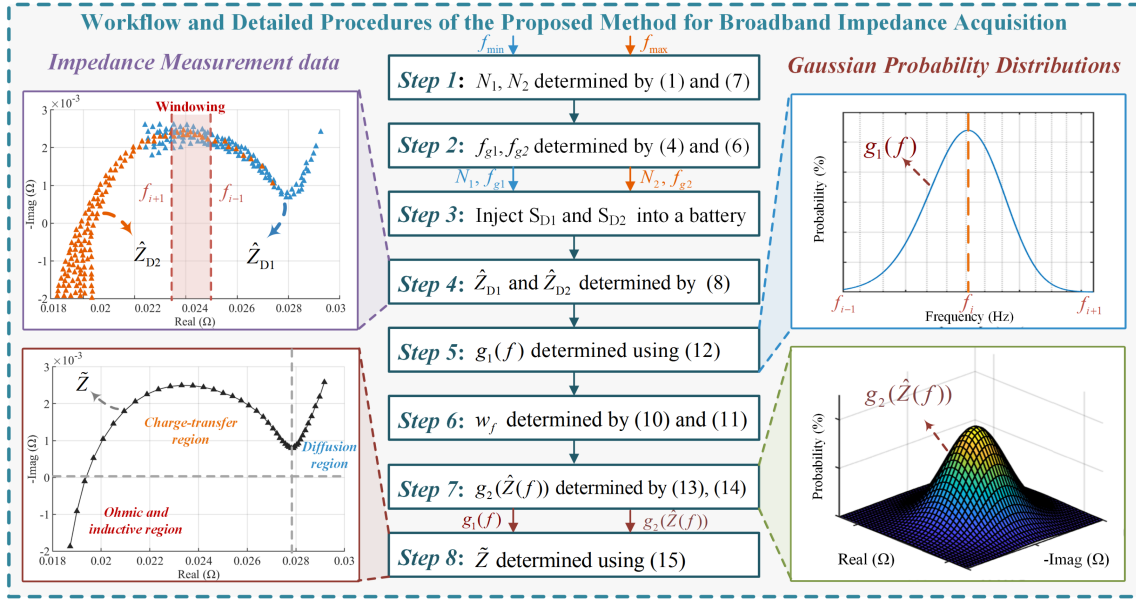


Fig. 4. Workflow and detailed procedures of the proposed method for measuring broadband battery impedance.

TABLE I
SPECIFICATIONS OF THE 18650 Li-ION BATTERIES

Cell name	Cell A	Cell B	Cell C
Nominal Voltage	3.60 V	3.60 V	3.60 V
Nominal Capacity	1.50 Ah	1.50 Ah	1.50 Ah
Present Capacity	1.53 Ah	1.26 Ah	1.11 Ah

The final form of impedance determination is represented as

$$\tilde{Z}(f_i) = \sum_{f=f_{i-1}}^{f_{i+1}} \hat{Z}(f) g_1(f) g_2(\hat{Z}_f) \left/ \sum_{f=f_{i-1}}^{f_{i+1}} g_1(f) g_2(\hat{Z}_f) \right. \quad (15)$$

where \hat{Z} and \tilde{Z} denote unfiltered and filtered impedance, respectively.

The workflow and detailed procedures of the proposed broadband battery impedance acquisition framework using the DPRS signal are summarized in Fig. 4.

IV. EXPERIMENTAL VALIDATION

A. Experimental Setup

The experimental studies are carried out on three 18650 Li-ion batteries to validate the proposed method on different SOCs, ambient temperatures, and aging status. The specifications of these batteries are listed in Table I. The battery test platform shown in Fig. 5 consists of a thermal chamber to regulate ambient temperature, a host computer to generate control signals, a bidirectional power supply to charge and discharge the battery, a data acquisition (DAQ) module to collect the measurements.

Considering battery impedance acquisition at very low frequencies is quite time-consuming, and the inductive impedance



Fig. 5. Experimental setup platform.

at very high frequencies only provides minor information, the investigated bandwidth ranges from $f_{\max} = 720$ Hz to $f_{\min} = 0.1$ Hz, which is capable of covering the most valuable information for estimating battery states [6], [10], [18], [26]. The specifications of the proposed DPRS signal are listed in Table II. According to (1) and (7), both S_{D1} and S_{D2} are designed as 255 bits. The generating frequencies are set as $f_{g1} = 25.5$ Hz and $f_{g2} = 1.6$ kHz, which are calculated by (4) and (6). The bandwidths of S_{D1} and S_{D2} are calculated as [0.1 Hz, 11.48 Hz] and [6.27 Hz, 720 Hz], respectively. Given the DPRS in this work has covered the investigated bandwidth ranging from 720 to 0.1 Hz very well, it is unnecessary to introduce additional subsequences that would prolong the signal injection period. The maximum sampling frequency f_s is selected as five times larger than f_{g2} . To avoid nonlinear distortion effects, the amplitude of the injection is an essential parameter that has to be carefully chosen. The guideline for the appropriate amplitude of the PRS signal is given in [23] ranging from 0.4 to 1 C. Given the batteries investigated in this work only have a

TABLE II
COMPARISON OF THE DPRS, PRS, AND SINE-SWEEP SIGNAL FOR BROADBAND BATTERY IMPEDANCE MEASUREMENTS

	DPRS signal	PRS signal	Sine-Sweep
f_{\max}	720 Hz	720 Hz	720 Hz
f_{\min}	0.1 Hz	0.1 Hz	0.1 Hz
f_s	8 kHz	8 kHz	-
f_{g1}	25.5 Hz	-	-
f_{g2}	1.6 kHz	1.6 kHz	-
N	255-bits	16383-bits	-
Signal level	+1 A, -1 A	+1 A, -1 A	Numerous
Injection time	10.16 s	10.2 s	37.9 s

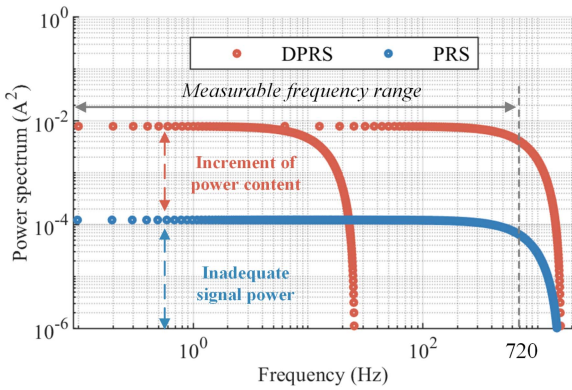


Fig. 6. Comparison of the DPRS and PRS signal in the frequency domain.

nominal capacity of 1.5 Ah, the amplitude of the DPRS is thus set to 1 A.

To highlight the superiority of the proposed DPRS signal, Table II compares the DPRS signal with the PRS and sine-sweep signal with the same frequency range. It is observed that the proposed DPRS method mitigates the signal injection time from 37.9 (Sine-sweep method) to 10.16 s, which is conducive to investigating dynamic electrochemical behaviors, real-time state estimation, and rapid failure detection. The DPRS signal and PRS signal have a similar injection time, while the DPRS signal significantly shortens the sequence's length from 16383 to 255 bits, which brings a substantial increment of signal power content and the reduction of the computing efforts to process the measurement data. Albeit the DPRS signal power content is about 64 times greater than that of the PRS signal as shown in Fig. 6, it is worth mentioning that it has the same amplitude of 1 A as the PRS signal in the time domain, which is a relatively small current excitation [11], [23] that would not excite the nonlinearities of the batteries.

B. Validation of the Proposed Method

We have tested *Cell A* in this section to verify the validity of the proposed method by comparing the traditional PRS method with a MAF for impedance filtering as in [23] and [24]. For

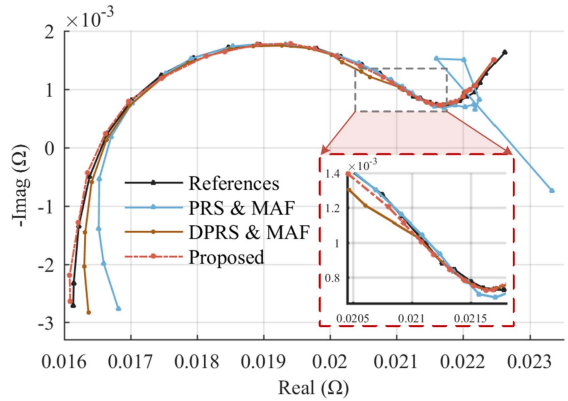


Fig. 7. Experimental results of broadband impedance acquisition for different methods.

controlling the variables, the specifications of the investigated DPRS signal and the PRS signal are the same as the ones given in Table I. The reference impedance curve is obtained by the sine-sweep method. The sweeping signals are made up of 30 frequency components with at least two periods (logarithmic ally ranging from 720 to 0.1 Hz), which are sequentially injected into the batteries in the form of current excitation with an amplitude of 0.1 C. In this section, the ambient temperature is set to 25 °C, while the battery SOC is 50%.

Fig. 7 plots the experimental results of broadband impedance acquisition using different methods. The PRS signal suffers from an insufficient SNR and sparse distribution of the harmonics in the low-frequency range that leads to poor frequency response accuracy to measure the Warburg diffusion impedance. In comparison, the proposed DPRS signal with a greatly enhanced power content is robust against interference and capable of achieving superior accuracy. The impedance measurement data obtained by the PRS and DPRS methods are respectively processed by the MAF for impedance filtering. Despite the impedance curves being smoothed, the MAF has a limited capability in dealing with the noise-induced impedance biases, the results are thus likely to deviate from the reference trajectory, especially in the high-frequency region. In contrast, the proposed WBIF with the consideration of signal power spectrum and impedance distribution characteristics can well handle the outliers with low probabilities, which enables more accurate and robust impedance results. Thanks to the outstanding properties of the well-designed DPRS signal and WBIF, the broadband impedance measurement results are quite close to the reference values in all frequency ranges. The effectiveness of the proposed broadband impedance acquisition framework is confirmed accordingly.

The normalized root mean square error (NRMSE) is selected to quantitatively analyze the impedance measurement accuracy as

$$\text{NRMSE} = \sqrt{\frac{1}{M} \sum_{i=1}^M \left(1 - \frac{Z_{\text{mea}}(i)}{Z_{\text{ref}}(i)} \right)^2} \quad (16)$$

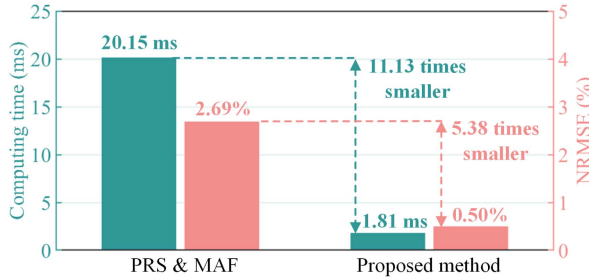


Fig. 8. Comparison of computing time and NRMSEs using different methods.

where M is the total number of impedance measurements, Z_{mea} is the measurement data, and Z_{ref} is the reference data.

The NRMSE of our proposed method is limited to merely 0.50%, while that of the DPRS & MAF and PRS & MAF methods have reached 0.84% and 2.69%, respectively. The accurate results confirm the superiority of the proposed DPRS and WBIF for the measurement of broadband battery impedance.

Further, we have verified the computing cost of the methods on a PC with MATLAB R2020a and a 2.80 GHz CPU. As shown in Fig. 8, our proposed method only requires 1.81 ms to process the measurement data, which is 11.13 times smaller than that of the PRS & MAF method. The above results confirm the superb accuracy and the easy-implementable property of the DPRS and the WBIF proposed in this work.

C. Validation on Different Battery SOCs, Ambient Temperatures, and Aging Status

Given battery impedance can be used for various states estimation as it closely relates to SOC, temperature variation, and aging status, we have further verified the feasibility and validity of the proposed method for battery impedance acquisition under various temperature, SOC, and aging conditions. In this work, we use *Cell A* to validate the proposed method under different temperatures and SOCs. Considering the degradation behavior of a battery is typically demonstrated by capacity loss, *Cell B* (1.26 Ah), and *Cell C* (1.11 Ah) can be further applied to simulate the aging behavior and degradation process of a battery.

The Nyquist plots of battery impedance measurements under different ambient temperatures (15, 25, and 35 °C) and battery SOCs (20%, 50%, and 80%) using different methods are presented in Fig. 9. The experimental results show that our proposed method can perfectly track the reference values all the time. The NRMSEs of battery impedance measurement results are shown in Fig. 10, where the average NRMSE of the PRS & MAF method is 1.83%, which is 2.95 times greater than that of our proposed method.

According to Fig. 9(a) and (b), the dependencies of battery impedance on SOC are mainly embodied in the medium- and low-frequency ranges. The semicircle in the medium-frequency range is dependent on the interfacial charge transfer reaction combined with the double-layer capacitance, and the straight line with an angle of 45° in the low-frequency region is related to the diffusion processes. The accurate results show our proposed

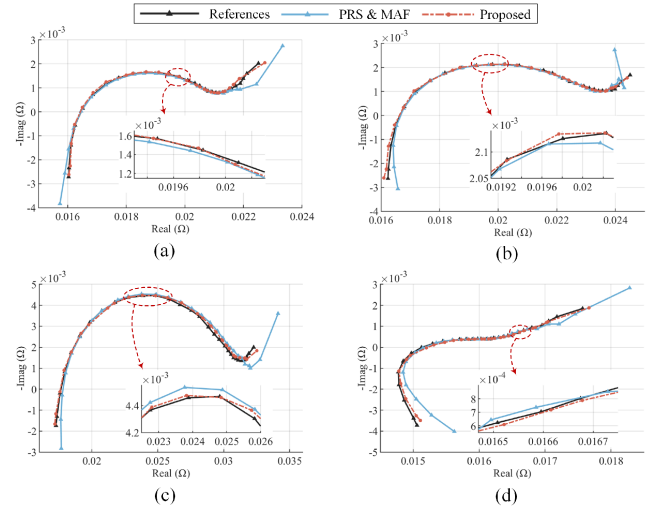


Fig. 9. Experimental results of the impedance measurements at (a) 80% SOC, 25 °C, (b) 20% SOC, 25 °C, (c) 50% SOC, 15 °C, (d) 50% SOC, 35 °C.

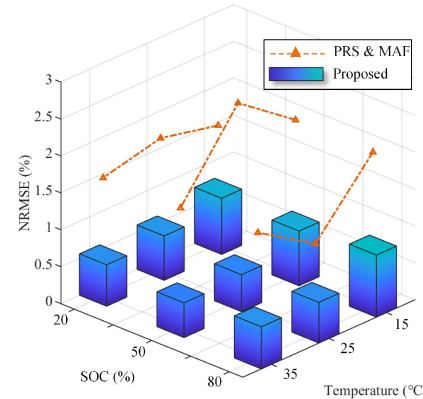


Fig. 10. Comparison of the NRMSEs using different methods.

method can well distinguish the medium- and low-frequency responses, the impedance results can thus be further used to identify the parameters of the equivalent circuit model (ECM) and estimate the battery SOC [26].

As shown in Fig. 11, the impedance spectra of new and aged cells basically are in the same shape. Nonetheless, for the aged cells, an additional semicircle can be observed in the high-frequency range. The phenomenon is caused by the solid electrolyte interface (SEI) forming on the surface of the anode due to the decomposition of the electrolyte [8]. Meanwhile, the other semicircle related to the charge-transfer reactions increases and shifts toward lower frequencies due to an increment of the time constant during cycling [7]. Meanwhile, the impedance measurement data yields strong negative dependencies over ambient temperatures, where both the real part and amplitude of battery impedance significantly shrink with the rising temperature, and the Ohmic resistance dominated by the electrolyte increases with decreasing temperature.

Through all the experimental studies in this work, the maximum NRMSEs of impedance measurements using our proposed

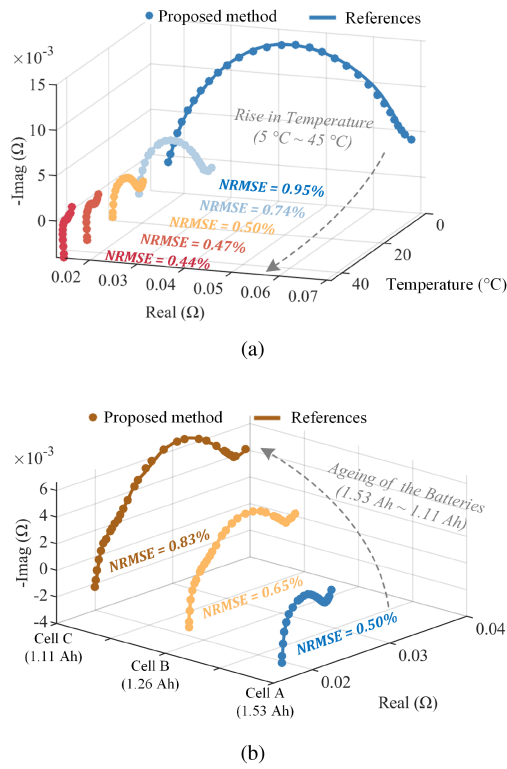


Fig. 11. Experimental results of battery impedance measurements at different (a) ambient temperatures ($5\text{--}45\text{ }^{\circ}\text{C}$) and (b) aging status (1.53–1.11 Ah).

method is limited to 0.95%. The nearly unbiased results confirm the validity and feasibility of the proposed method under various operating conditions including ambient temperatures, SOCs, and the aging status of the batteries. Therefore, it is believed that the proposed fast broadband impedance acquisition framework is conducive to future impedance-based state estimation for online applications.

V. CONCLUSION

PRS signal enabled a fast and low-complexity broadband battery impedance acquisition but at the expense of an inadequate SNR, which further led to an easily biased result. This article thus proposed a novel DPRS signal, where two subsequences were connected in series and carried out on different scales for acquiring broadband battery impedance. The DPRS signal notably improved the signal power content in all frequency ranges, where the high-fidelity impedance measurement data were particularly robust against interference. The WBIF carried out on a semilogarithmic scale suppressed the noise disturbances and compensated for the noise-induced biases, which enabled a nearly unbiased result.

Experimental studies confirmed the superiority of the proposed method under various SOCs, ambient temperatures, and the aging status of three Li-ion batteries. The proposed DPRS signal only took 10.16 s to measure broadband battery impedance with frequencies ranging from 720 to 0.1 Hz. In

comparison with the sine-sweep signal, 73% of the signal injection time can be saved. 91% of the computing efforts can be saved compared to the PRS and MAF method. The proposed method kept tracking the reference all the time, where the maximum NRMSEs were limited to 0.95% through all the tests.

Future works focus on the feasibility of the proposed method for measuring the battery impedance during operating conditions.

REFERENCES

- [1] X. Du et al., “An information appraisal procedure: Endows reliable online parameter identification to Lithium-ion battery model,” *IEEE Trans. Ind. Electron.*, vol. 69, no. 6, pp. 5889–5899, Jun. 2022.
- [2] Z. Wei, J. Hu, H. He, Y. Li, and B. Xiong, “Load current and state-of-charge coestimation for current sensor-free Lithium-ion battery,” *IEEE Trans. Power Electron.*, vol. 36, no. 10, pp. 10970–10975, Oct. 2021.
- [3] D. Chen et al., “An empirical-data hybrid driven approach for remaining useful life prediction of Lithium-ion batteries considering capacity diving,” *Energy*, vol. 245, 2022, Art. no. 123222.
- [4] Z. Wei, G. Dong, X. Zhang, J. Pou, Z. Quan, and H. He, “Noise-immune model identification and state-of-charge estimation for lithium-ion battery using bilinear parameterization,” *IEEE Trans. Ind. Electron.*, vol. 68, no. 1, pp. 312–323, Jan. 2021.
- [5] J. Kim and J. Kowal, “A method for monitoring state-of-charge of lithium-ion cells using multi-sine signal excitation,” *Batteries*, vol. 7, no. 4, 2021, Art. no. 76.
- [6] C. T. Love, M. B. Virji, R. E. Rocheleau, and K. E. Swider-Lyons, “State-of-health monitoring of 18650 4S packs with a single-point impedance diagnostic,” *J. Power Sources*, vol. 266, pp. 512–519, 2014.
- [7] W. Waag, S. Käbitz, and D. U. Sauer, “Experimental investigation of the lithium-ion battery impedance characteristic at various conditions and aging states and its influence on the application,” *Appl. Energy*, vol. 102, pp. 885–897, 2013.
- [8] K. Mc Carthy, H. Gullapalli, K. M. Ryan, and T. Kennedy, “Review-use of impedance spectroscopy for the estimation of Li-ion battery state of charge, state of health and internal temperature,” *J. Electrochem. Soc.*, vol. 168, no. 8, 2021, Art. no. 080517.
- [9] R. Mingant et al., “EIS measurements for determining the SOC and SOH of Li-ion batteries,” *ECS Meeting Abstr.*, vol. MA2010-02, no. 4, pp. 213–213, 2010.
- [10] B. G. Carkhuff, P. A. Demirev, and R. Srinivasan, “Impedance-based battery management system for safety monitoring of Lithium-ion batteries,” *IEEE Trans. Ind. Electron.*, vol. 65, no. 8, pp. 6497–6504, Aug. 2018.
- [11] J. Zhu, Z. Sun, X. Wei, and H. Dai, “Studies on the medium-frequency impedance ARC for Lithium-ion batteries considering various alternating current amplitudes,” *J. Appl. Electrochem.*, vol. 46, no. 2, pp. 157–167, 2016.
- [12] M. Koseoglou, E. Tsiontas, D. Ferentinou, N. Jabbour, D. Papagiannis, and C. Mademlis, “Lithium plating detection using dynamic electrochemical impedance spectroscopy in Lithium-ion batteries,” *J. Power Sources*, vol. 512, 2021, Art. no. 230508.
- [13] Z. Xia and J. A. Abu Qahouq, “Adaptive and fast state of health estimation method for Lithium-ion batteries using online complex impedance and artificial neural network,” in *Proc. IEEE Appl. Power Electron. Conf. Expo.*, 2019, pp. 3361–3365.
- [14] L. H. Raijmakers, D. L. Danilov, J. P. Van Lammeren, M. J. Lammers, and P. H. Notten, “Sensorless battery temperature measurements based on electrochemical impedance spectroscopy,” *J. Power Sources*, vol. 247, pp. 539–544, 2014.
- [15] J. Jiang, H. Ruan, B. Sun, L. Wang, W. Gao, and W. Zhang, “A low-temperature internal heating strategy without lifetime reduction for large-size automotive lithium-ion battery pack,” *Appl. Energy*, vol. 230, pp. 257–266, 2018.
- [16] E. Din, C. Schaeff, K. Moffat, and J. T. Stauth, “A scalable active battery management system with embedded real-time electrochemical impedance spectroscopy,” *IEEE Trans. Power Electron.*, vol. 32, no. 7, pp. 5688–5698, Jul. 2017.

- [17] M. Koseoglou, E. Tsiontas, D. Papagiannis, N. Jabbour, and C. Mademlis, "A novel on-board electrochemical impedance spectroscopy system for real-time battery impedance estimation," *IEEE Trans. Power Electron.*, vol. 36, no. 9, pp. 10776–10787, Sep. 2021.
- [18] J. G. Zhu, Z. C. Sun, X. Z. Wei, and H. F. Dai, "A new Lithium-ion battery internal temperature on-line estimate method based on electrochemical impedance spectroscopy measurement," *J. Power Sources*, vol. 274, pp. 990–1004, 2015.
- [19] A. D. Angelis, E. Buchicchio, F. Santoni, A. Moschitta, and P. Carbone, "Practical broadband measurement of battery EIS," in *Proc. IEEE Int. Workshop Metrol. Autom., MetroAutomotive*, 2021, pp. 25–29.
- [20] X. Wang, Y. Kou, B. Wang, Z. Jiang, X. Wei, and H. Dai, "Fast calculation of broadband battery impedance spectra based on S transform of step disturbance and response," *IEEE Trans. Transport. Electricif.*, vol. 8, no. 3, pp. 3659–3672, Sep. 2022.
- [21] Q. Yao, D. Lu, and G. Lei, "Battery impedance measurement using fast square current perturbation," in *Proc. IEEE 4th Int. Future Energy Electron. Conf.*, 2019, pp. 1–5.
- [22] A. H. Tan and K. R. Godfrey, "The generation of binary and near-binary pseudorandom signals: An overview," *IEEE Trans. Instrum. Meas.*, vol. 51, no. 4, pp. 583–588, Aug. 2002.
- [23] J. Sihvo, D. I. Stroe, T. Messo, and T. Roinila, "A fast approach for battery impedance identification using pseudo-random sequence signals," *IEEE Trans. Power Electron.*, vol. 35, no. 3, pp. 2548–2557, Mar. 2020.
- [24] J. Sihvo, T. Roinila, and D. I. Stroe, "Novel fitting algorithm for parametrization of equivalent circuit model of li-ion battery from broadband impedance measurements," *IEEE Trans. Ind. Electron.*, vol. 68, no. 6, pp. 4916–4926, Jun. 2021.
- [25] J. A. Qahouq and Z. Xia, "Single-perturbation-cycle online battery impedance spectrum measurement method with closed-loop control of power converter," *IEEE Trans. Ind. Electron.*, vol. 64, no. 9, pp. 7019–7029, Sep. 2017.
- [26] X. Wang et al., "A review of modeling, acquisition, and application of Lithium-ion battery impedance for onboard battery management," *eTransportation*, vol. 7, 2021, Art. no. 100093.
- [27] K. R. Godfrey, H. A. Barker, and A. J. Tucker, "Comparison of perturbation signals for linear system identification in the frequency domain," *IEE Proc., Control Theory Appl.*, vol. 146, no. 6, pp. 535–548, 1999.
- [28] T. Sun, S. Gawad, C. Bernabini, N. G. Green, and H. Morgan, "Broadband single cell impedance spectroscopy using maximum length sequences: Theoretical analysis and practical considerations," *Meas. Sci. Technol.*, vol. 18, no. 9, pp. 2859–2868, 2007.
- [29] B. Liebhart, S. Diehl, D. Schneider, C. Endisch, and R. Kennel, "Enhancing the cell impedance estimation of a Lithium-ion battery system with embedded power path switches," in *Proc. IEEE Appl. Power Electron. Conf. Expo.*, 2021, pp. 967–974.
- [30] K. Godfrey, "Design and application of multifrequency signals," *Comput. Control Eng. J.*, vol. 2, no. 4, pp. 187–195, 1991.
- [31] M. Elad, "On the origin of the bilateral filter and ways to improve it," *IEEE Trans. Image Process.*, vol. 11, no. 10, pp. 1141–1151, Oct. 2002.



Xinghao Du received the B.S. degree in electrical engineering from Civil Aviation Flight University of China, Deyang, China, in 2020. He is currently working toward the M.S. degree in electrical engineering with the College of Electrical Engineering, Sichuan University, Chengdu, China.

His current research interests include lithium-ion battery modeling, states estimation, and broadband impedance applications.



Jinhao Meng (Member, IEEE) received the M.S. degree in control theory and control engineering and the Ph.D. degree in electrical engineering from the Northwestern Polytechnical University (NPU), Xi'an, China, in 2013 and 2019, respectively.

He is currently an Associate Professor in Xi'an Jiaotong University, Xi'an. His research interests include battery modeling, battery states estimation, and energy management of battery energy storage systems.



Jichang Peng received the B.S. degree in electrical engineering from the North China University of Water Resources and Electric Power, Zhengzhou, China, in 2010, and the M.S. degree in control theory and control engineering and the Ph.D. degree in electrical engineering from Northwestern Polytechnical University, Xi'an, China, in 2013 and 2019, respectively.

He is currently a Lecturer in Nanjing Institute of Technology, Nanjing, China. His research interests include battery modeling, energy management, and aircraft starter/generator and sensorless control of brushless synchronous machine.



Youbo Liu (Member, IEEE) received the B.Sc., M.Sc., and Ph.D. degrees from Sichuan University, Chengdu, China, in 2005, 2008, and 2011, respectively.

He is currently an Associate Professor with the College of Electrical Engineering and Information Technology, Sichuan University. His research interests include machine learning in smart grid and energy-storage system applications.